



Characteristics of rootless cone tephra emplaced by high-energy lava–water explosions

Erin P. Fitch¹ · Sarah A. Fagents²

Received: 9 September 2019 / Accepted: 3 June 2020 / Published online: 29 July 2020
© International Association of Volcanology & Chemistry of the Earth's Interior 2020

Abstract

The effects of external water during hydrovolcanic eruptions are difficult to quantify; however, research investigating the explosive interactions between surface lava flows and water has provided new insights into explosion dynamics. Previous work has focused on relatively low-energy lava–water explosions from a 100-m-diameter cone in the Rauðhólar cone group in Iceland. For comparison, we study ejecta derived from higher-energy explosions at the 400-m-diameter Pu‘u Kīholo rootless cone in Hawai‘i, one of the largest rootless cones on Earth. This comparative approach elucidates the effect of lava–water mixing conditions and range of explosivity on ejecta characteristics. Utilizing grain size analysis, we found that Pu‘u Kīholo beds typically have median grain sizes at the cone rim that are smaller than -3ϕ (8 mm) and are on average finer-grained than those of the Rauðhólar cone. Ash-sized grains, the most energetically significant ejecta size fraction, typically make up $> 20\%$ of bed ejecta, with a maximum of 90%, both greater proportions than found in beds of the Rauðhólar cone. Utilizing grain morphology, crystal texture, and surface feature analysis, we found that the abundance of ash-sized grains associated with high heat transfer rates (i.e., active particles) increases at Pu‘u Kīholo as explosivity increases, which is an important consideration for energy modeling. This dataset also includes ejecta from the finest-grained beds, and therefore highest-energy lava–water explosions, studied to date.

Keywords Hydrovolcanic · Phreatomagmatic · Magma–water · Molten fuel–coolant interaction · Littoral

Introduction

It is important to understand how external water increases the energetics of phreatomagmatic eruptions to build effective models for hazard assessment. However, explosive magma–water interactions are difficult to quantify because juvenile volatiles are also a factor in explosive energetics, and both external water and internal gases within the magma contribute to the generation and dispersal of tephra (e.g., Houghton and Hackett 1984; Houghton and Schmincke 1986; Morrissey et al. 2000; Zimanowski 2001; Wohletz et al. 2013).

The inferred explosion mechanism associated with magma–water interactions, molten fuel–coolant interaction (MFCI; outlined in Fig. 1; Colgate and Sigurgeirsson 1973), has been simulated in lab-scale to field-scale experiments (e.g., Wohletz and McQueen 1981, 1984; Wohletz 1983, 1986; Lorenz 1987; Zimanowski et al. 1997a; Büttner et al. 1999; Büttner et al. 2002; Sonder et al. 2018). MFCI explosion energy is proportional to the energy required to produce finely fragmented grains, termed “active” (or “interactive”) particles (Büttner and Zimanowski 1998; Büttner et al. 2002).

Interactions between largely outgassed lava flows and water can also be explosive and produce “rootless” cones. Rootless cones therefore provide a natural analog to MFCI experiments, which typically use outgassed, re-melted tephra, or lava fragments. As lava–water explosivity increases, melt fragmentation and ejecta dispersal increases, producing finer-grained beds and rootless cones with larger diameters (Greeley and Fagents 2001; Fitch et al. 2017; Hamilton et al. 2017). Rootless cones range from 2 to 450 m in diameter (Fagents and Thordarson 2007). Here, we investigate the stratigraphy and ejecta characteristics of the ~ 400 -m-diameter

Editorial Responsibility: P-S. Ross

✉ Erin P. Fitch
epfitch@higp.hawaii.edu

¹ Department of Earth Sciences, University of Hawai‘i, 1680 East-West Road, Honolulu, HI 96822, USA

² Hawai‘i Institute of Geophysics and Planetology, University of Hawai‘i, Honolulu, HI, USA

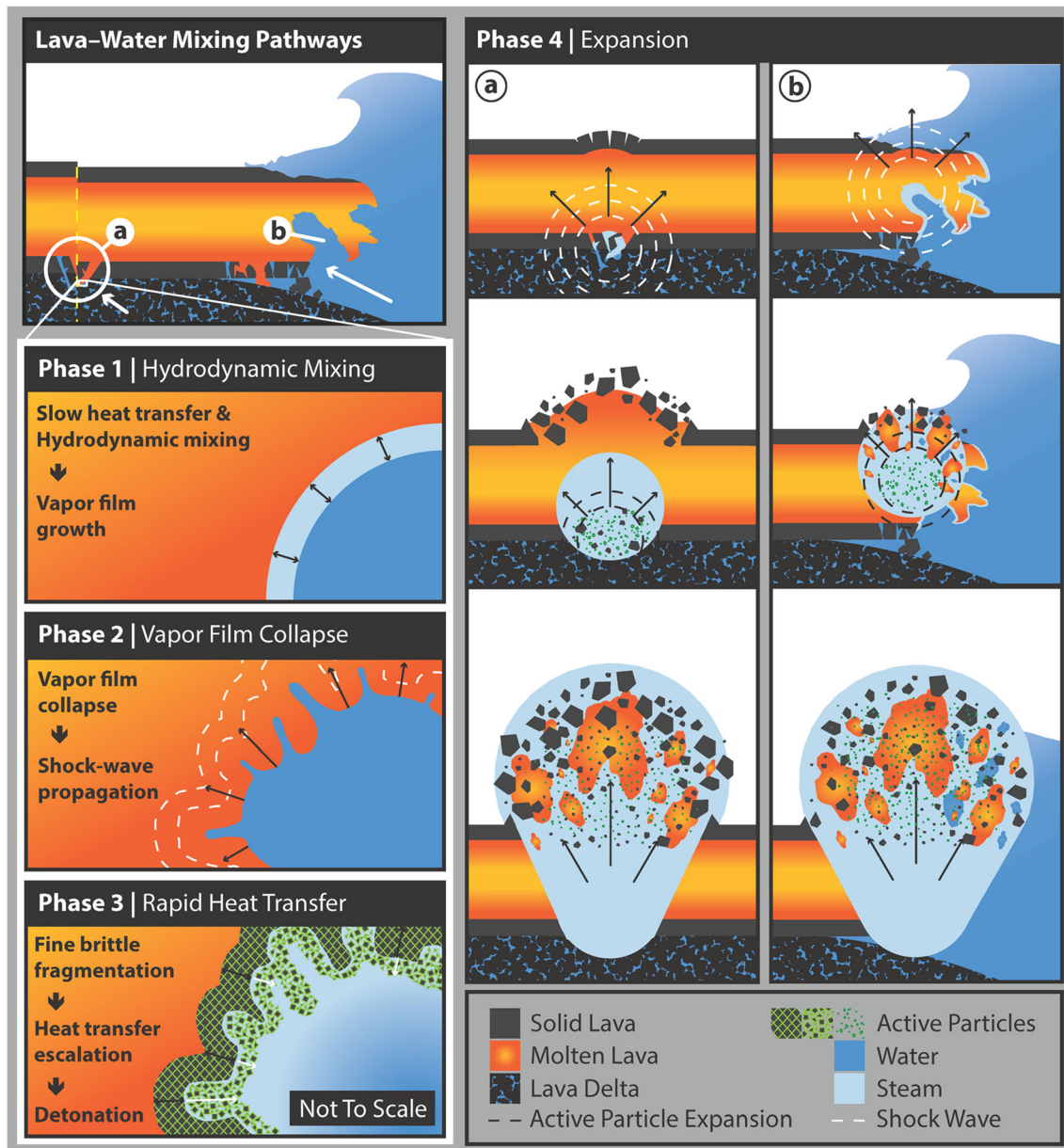


Fig. 1 Littoral lava–water mixing pathways may be (a) confined, where fracturing of the flow basal crust allows lava to mix with water within the substrate pore space, or (b) open, where wave action forces mixing directly with the molten flow core. An MFCEI explosion may then occur by initial hydrodynamic (ductile) mixing and development of a vapor film between the melt and water (phase 1), followed by a collapse of the vapor

film and propagation of stress waves through the cooling melt (phase 2), with subsequent deformation and initiation of fine fragmentation and escalating heat transfer at the finely fragmented lava–water interface (phase 3), with final vaporization of the water and expansion through the melt (phase 4)

littoral Pu‘u Kīholo rootless cone in Hawai‘i and compare our results with a previously studied ~100-m-diameter lacustrine rootless cone in the Rauðhólar cone group in Iceland (Fitch et al. 2017; Hamilton et al. 2017).

Beds from these two cones likely formed over a wide range of lava–water explosion energies and we compare them to determine (1) the range of grain size distributions present and (2) the relationship between the median grain size of beds

and other characteristics indicative of explosion energy, such as the mass percentage of ash-sized grains and active particles (Büttner and Zimanowski 1998; Büttner et al. 2002). Since Pu‘u Kīholo cone has a diameter close to the maximum known for rootless cones, this work provides an opportunity to highlight the characteristics of ejecta formed during high-energy explosions. These cones formed in different settings and are associated with different lava flow types, so the effects

of differing (1) lava–water mixing conditions and (2) lava flow properties on the characteristics of ejecta are also investigated. Therefore, this work provides a comparative dataset that elucidates the conditions under which lava–water explosions are generated, their qualitative range of explosivity, and how explosion setting affects ejecta characteristics. These data are important inputs for the estimation of lava–water explosivity (energy per unit mass of ejecta), which may be similar to the explosion energy of MFCI experiments and explosive magma–water interactions.

Study areas

Within the Rauðhólar rootless cone group located outside of Reykjavík, Iceland, a cone designated “cone 53” (64.094893° N, 21.751814° W) by von Komorowicz (1912), was studied in detail by Fitch et al. (2017) and Hamilton et al. (2017). It is inferred to have once had a basal diameter of approximately 100 m, based on a regional map made before it was quarried, and it has an approximately 60-m crater diameter. It is associated with a tube-fed pāhoehoe flow and lava–water interaction was inferred to have initiated by cracking of the basal crust of the flow, which allowed molten lava to come into contact with water-saturated lake sediment (Fagents and Thordarson 2007; Hamilton et al. 2017). A proximal 14-m-high section was studied and divided into 68 beds, 97% of which are dominated by bomb- to lapilli-sized clasts. We hereby refer to this study site as “Rauðhólar.”

In comparison with the Rauðhólar cone, this study presents new data for Pu‘u Kīholo cone (19.020493° N 155.839506° W), a large rootless cone in the Na Pu‘u a Pele littoral rootless cone group in the Manukā Natural Area Reserve, on the southern flank of Mauna Loa on the island of Hawai‘i. Lava flows were emplaced during and after cone formation and they partly obscure the cone morphology. However, based on the location of lava pressure ridges and ponding high-stand levels, we infer that it has a basal diameter of approximately 400 m, and a 314-m crater diameter (Fig. 2). The northwest cone flank is twice as high and wide as the southeast flank, a characteristic common to three other cones in the group. This is likely the result of tephra dispersal in winds from the east and southeast, which are prevalent in this region (Xie et al. 2001).

The Na Pu‘u a Pele littoral rootless cone group is associated with the Hapai manu lava flows, approximately 240 ± 60 years old, generated by Mauna Loa flank eruptions from 1650-m- and 1950-m-elevation vents (Trusdell and Lockwood in press). These flows are recorded in a Hawaiian story in which the goddess Pele sent lava flows down the southern slopes of Mauna Loa, overwhelming two chiefs near the coast, who are immortalized as the two halves of Na Pu‘u a Pele cone (Westervelt 1916). Flows likely reached the coast within a week based on the presence of wide channels, voluminous

rubbly pāhoehoe flows, and large ‘a‘ā flows with pressure ridges, analogous to the 1960 Kapoho flows (Rowland and Walker 1987). Many flows were confined on the coast behind topographic barriers or impeded by shallower slopes. These flows ponded, and then released, resulting in some flows entering the ocean at high fluxes, making explosive mixing more likely (Jurado-Chichay et al. 1996).

Methods

Stratigraphy and grain size analysis

To compare deposit characteristics between Rauðhólar and Pu‘u Kīholo cones, we sampled at the crater rim, following Sheridan and Wohletz (1983), at a radial section through the southeast cone flank of Pu‘u Kīholo. We chose a 4.2-m-high section, 159 m from the cone center, which is the closest location to the crater rim that does not overlap a slumped portion of the exposed cone (Fig. 3). The section comprises 17 fall beds and the uppermost three are also found at shallow exposures into the surface around the entire cone.

Representative samples of each bed were taken, such that no individual clast weighed $> 5\%$ of the total sample weight. Medium bomb-sized clasts (-8 to -7ϕ ; 256–128 mm) were measured by hand and fine bomb- to coarse-lapilli-sized clasts (-7 to -4ϕ ; 128–16 mm) were sieved at 1 ϕ intervals. Medium lapilli- to very fine ash-sized clasts (-4 to 4ϕ ; 16 to 62 μm) were sieved using standard equipment and methods at 0.5 ϕ intervals. For beds containing $> 5\%$ material $< 4 \phi$ ($< 62 \mu\text{m}$), the extremely fine ash component was analyzed using a Horiba Partica LA-950V2 laser diffraction particle size analyzer and calibrated using a basaltic refractive index of 1.66, following Horwell (2007). Results were adjusted to reflect a dried sample weight and grain size statistics were calculated by the Folk and Ward (1957) method using the GRADISTAT program (Version 8), as recommended by Blott and Pye (2001).

Ejecta morphology and secondary fragmentation

The resulting morphologies of lava–water explosion ejecta are dependent on the rheology and stress state of the lava at the time of fragmentation (Fig. 4(a)). *Blocky* and *shard-like* morphologies result from brittle fragmentation of solid lava, or molten lava that underwent high strain rates at the lava–water interface (Dürig et al. 2012; Fitch et al. 2017). *Fluidal* morphology results from hydrodynamic (ductile) fragmentation when surface tension effects dominate melt behavior (Wohletz 1983) during phase 4 expansion (Mattox and Mangan 1997; Zimanowski et al. 1997a; Fitch et al. 2017). *Spinose*, or viscous, morphology also forms due to hydrodynamic fragmentation, where viscous effects dominate melt behavior over surface tension effects, producing irregular

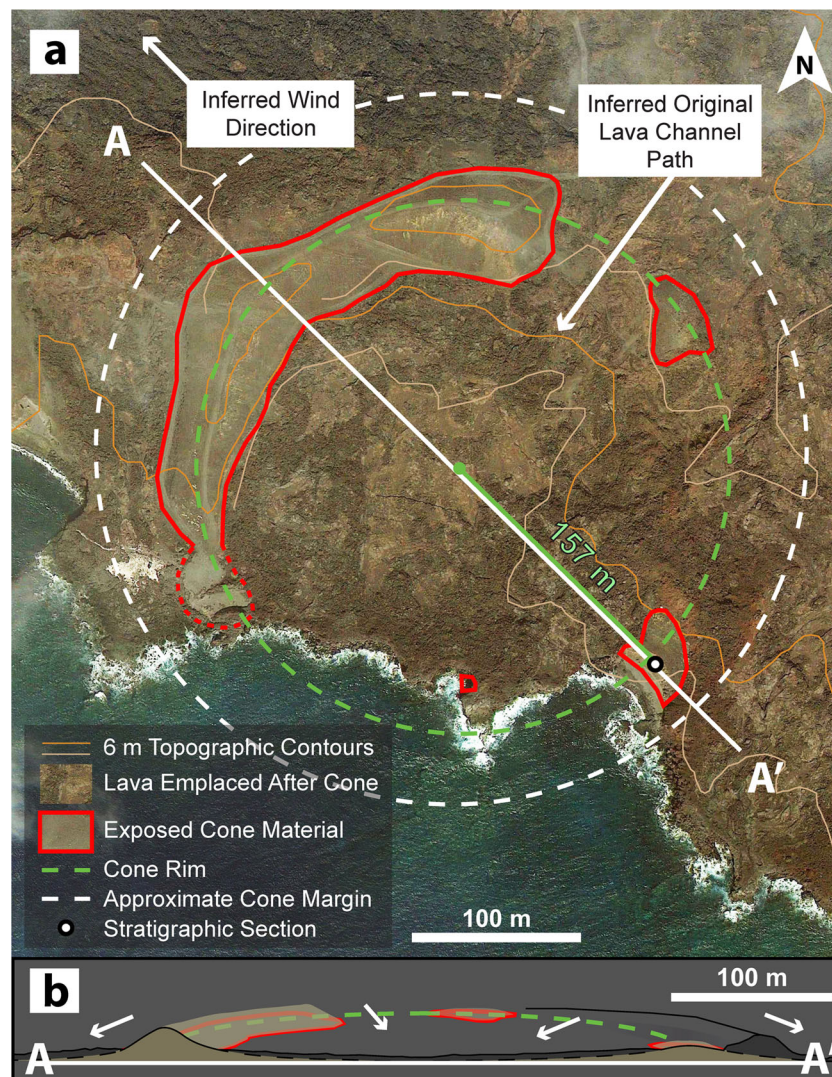


Fig. 2 (a) The estimated margins and crater of Pu'u Kiholo cone. The stratigraphic section lies in the medial section of the cone, 2 m from the crater rim. (b) The profile from A to A' shows the inferred cone geometry (to scale) as well as an oblique perspective north of the profile

clasts similar to 'a'a clinker (Harris and Rowland 2015). However, irregularly shaped *mossy* ash-sized grains are composed of annealed smaller particles formed at the melt–water

interface and are therefore considered a form of an active particle (Wohletz 1983; Zimanowski et al. 2015). Note that previously, Fitch et al. (2017) use the term “mossy” to broadly

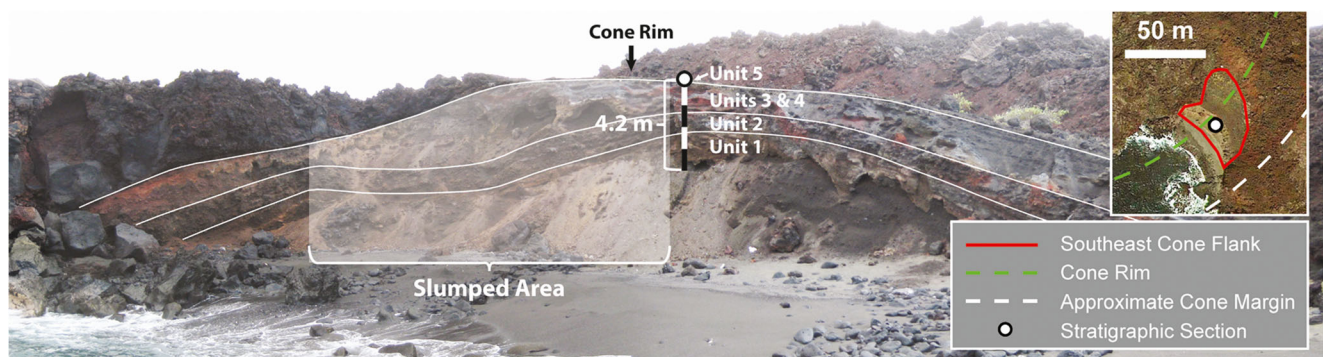


Fig. 3 The southeast flank radial exposure of Pu'u Kiholo cone. Measurements indicate the beds thin consistently in the distal direction, although they appear thicker in the photograph because they are closer to the viewer. The inset image displays the southeast flank in an aerial view

describe all clasts formed during a rheology regime dominated by viscous effects, encompassing the grains we classify separately as “spinose” and “mossy” in this work.

We classified 100 clasts from each of the bomb and lapilli grain sizes of each bed as blocky, spinose, or fluidal. For beds where bomb-sized clasts (-8 to -6ϕ ; 256 to 64 mm) make up $>10\%$ by mass, we visually estimated morphology percentages in the field. We classified 100 lapilli-sized clasts from -5 to -4ϕ (32–16 mm) and from -4 to -3ϕ (16–8 mm) which were present in sufficient quantities. For finer-grained beds 1.3 and 1.5 (Fig. 5), we analyzed 100 clasts from the -2 to -1ϕ (4–2 mm) and -1 to -0.5ϕ (2–1.4 mm) bins, respectively. We classified ash-sized grains as blocky, fluidal, spinose, or mossy (Fig. 4(a,e)), shard-like, aggregate, or free crystals, following Heiken and Wohletz (1985) and Fitch et al. (2017) (except bed 4.1). For each bed, 100 juvenile grains were analyzed from each of three size bins: $0.5-0 \phi$ (1.41–1.00 mm, very coarse ash), $1.5-2 \phi$ (0.354–0.250 mm, medium ash), and $3.5-4 \phi$ (88–62 μm , very fine ash).

Following Fitch et al. (2017), we calculated the total mass percentage of ejecta classified as blocky, spinose, and fluidal, using the results of morphology analysis. Morphologies that make up a minor portion of the ejecta mass, such as mossy and shard-like ash are not included. For bomb-sized ejecta (-8 to -6ϕ ; 256–64 mm), we use field estimates of bomb percentage where possible, and lapilli morphology analysis for beds where field analysis of bomb-sized clasts could not be made reliably because they make up $<10\%$ of the ejecta mass. For lapilli-sized ejecta (-6 to -1ϕ ; 64–2 mm), we use the medium lapilli (-4 to -3ϕ ; 16–8 mm) morphology analysis, except for the following beds that did not contain enough medium lapilli to analyze: bed 5.2 ($0.5-0 \phi$; 1.41–1.00 mm; 100 grains), 4.1 (-5 to -4ϕ ; 32–16 mm; 25 clasts total), 1.5 (-2 to -1ϕ , 100 clasts), and 1.3 (-1 to -0.5ϕ , 100 clasts). For ash-sized ejecta, we use the average morphology percentage over the three ash size bins analyzed. For each size range, we multiplied the percentage of each morphology by the mass percentage of ejecta within that size range for each bed in order to obtain the total mass percentage of each morphology for each bed.

Secondary fragmentation of ejecta, due to grain collisions within the expanding, turbulent gas–particle envelope (Mastin 2007) or upon deposition, may be more prevalent in higher-energy explosions. Therefore, we also estimated the percentage of fluidal clasts that are highly abraded and/or fragmented, defined as retaining less than 50% of the original fluidal surface area, to assess the degree of secondary fragmentation. However, any grain that displays a fluidal surface, even if it is not the dominant morphology, was still classified as “fluidal.”

Ejecta crystal textures and surface features

Of particular interest is the abundance of active particles, which are defined as blocky and mossy grains smaller than 3

ϕ , (125 μm), where blocky grains have distinctive surface features such as polygonal quench cracks (sometimes known as branching quench cracks) and stepped features (Fig. 4(f,g)) (e.g., Heiken and Wohletz 1985; Wohletz 1986; Büttner et al. 1999, 2002; Zimanowski et al. 2015). Active particles are sourced from the molten flow interior and cool quickly, resulting in a glassy groundmass, which distinguishes them from blocky, crystalline lithics (Büttner et al. 2002), such as grains sourced from lava crust. Therefore, we identified the crystal textures (an indication of cooling rates) associated with (1) molten lava and solid crust samples, and (2) polished sections of 100 ash-sized grains from each of three size bins: $0.5-0 \phi$ (1.41–1.00 mm, very coarse ash), $1.5-2 \phi$ (0.354–0.250 mm, medium ash), and $3.5-4 \phi$ (88–62 μm , very fine ash), for each bed except 4.1, where the abundance of ash could not be determined. With a scanning electron microscope (SEM) using backscatter imagery (BSE) of carbon tape grain mounts, we also analyzed the abundance of surface pitting caused by alteration by hydrothermal fluids (Fig. 4(h)), stepped features caused by intensive brittle fracturing, and polygonal quench cracks over 50 blocky ash-sized grains from each of the same three size bins as crystal texture analysis, for select beds. We then estimated the mass percentage of active particles of select beds using (1) size (we anticipate grains $<2 \phi$, but also analyzed grains up to 0ϕ), (2) morphology (blocky or mossy), (3) crystal texture (hypocrystalline), and (4) surface features (quench cracks and stepped features).

Lapilli vesicularity and component analysis

Ejecta from rootless cones include clasts sourced from lava crust, the molten core of the flow, and a minor component of free crystals. The relative abundance of these components is dependent on the rheology of lava at the time of fragmentation and the degree and style of explosive lava–water interaction (Mattox and Mangan 1997; Fitch et al. 2017). The characteristics of ejecta sourced from the solid crust, termed “lava lithics,” were constrained at Pu‘u Kīhōlo by comparing the vesicle characteristics of ejecta with (1) those of the surrounding Hapaimanu lava flows and (2) easily identifiable blocky lava lithics from a small, unnamed spatter-dominated rootless cone (located at 19.02352° N, 155.85535° W) within the Na Pu‘u a Pele cone group. We measured the density of the characteristic (i.e., archetypal) lava lithics from these two sources, in addition to 395 randomly selected lapilli from five Pu‘u Kīhōlo beds, 1.1, 2.1, 3.3, 3.5, and 4.1, following standard methods outlined in Houghton and Wilson (1989) and also applied by Fitch et al. (2017). Density was converted to vesicularity using a dense rock equivalent (DRE) value of 2910 kg m^{-3} , our highest measured density. A comparison of clasts from these three sources allows us to constrain the lava flow type associated with lava lithics within Pu‘u Kīhōlo beds.

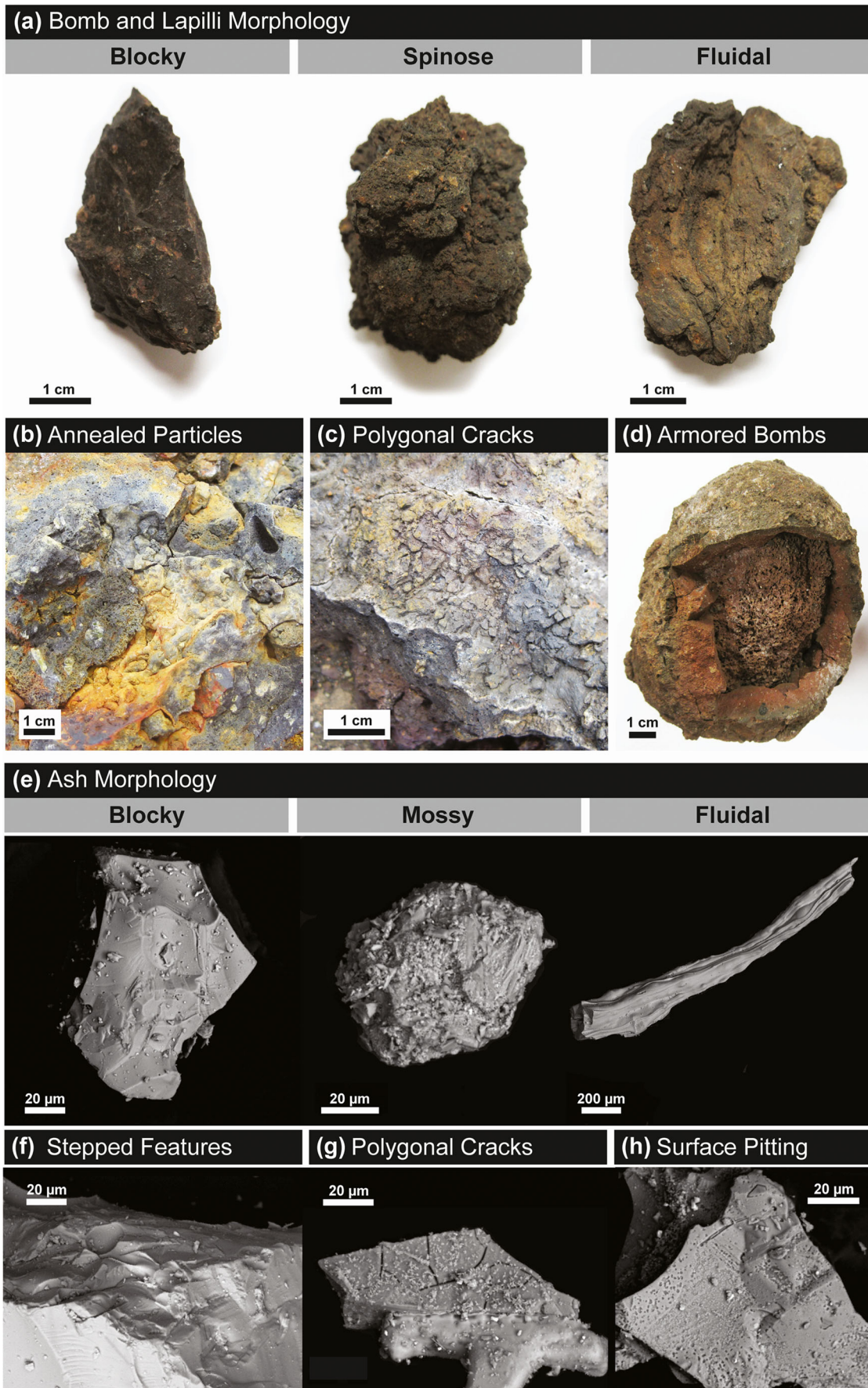


Fig. 4 (a) Blocky, spinose, and fluidal morphologies of bomb and lapilli-sized ejecta at Pu‘u Kīhōlo cone. (b) Annealed and partially incorporated grains ≤ 10 cm in diameter. (c) Local shallow polygonal cracks on the surface of a fluidal bomb. (d) An armored bomb composed of a vesicular lava-lithic block surrounded by dense material sourced from molten lava. (e) Blocky, mossy, and fluidal morphologies of ash-sized ejecta at Pu‘u Kīhōlo cone and associated surface features: (f) stepped features associated with active particles, (g) polygonal quench cracks, (h) chemical surface pitting

Statistical correlation

Following Fitch et al. (2017), we interpret the coefficient of determination (r^2) values between datasets from 0 to 0.30 as a negligible correlation, 0.31 to 0.50 as a weak correlation, 0.51 to 0.70 as a moderate correlation, and 0.71 to 1.00 as a strong correlation. For example, a strong correlation occurs if more than 70% of the variance in the dataset can be accounted for by the model.

Results

Stratigraphy and grain size analysis

We group beds into five separate stratigraphic units based on the grain size distributions of the beds. Specifically, there are two very coarse units, numbers 2 and 4, with modal grain sizes between -8 and -7ϕ , and three finer units, numbers 1, 3, and 5, with modal grain sizes between -3 and 3ϕ (Fig. 5). Explosive activity occurred near the Pu‘u Kīhōlo cone center, as evidenced by beds at the study section thinning away from it, and the lack of other cone centers within 650 m northwest of the study section. Beds are gray but display minor yellow or red portions that do not follow bedding planes and likely reflect secondary alteration due to water vapor rising through the beds of cooling ejecta. Beds commonly contain annealed and/or embedded ash- to lapilli-sized grains (Fig. 4(b)) on the surfaces of larger clasts, in particular beds 2.1 and 4.1, because they contain a large percentage of fluidal, bomb-sized ejecta. These beds also contain notable armored bombs (Fig. 4(d)), which commonly display localized shallow polygonal cracks on their otherwise fluidal surfaces (Fig. 4(c)), which are inferred to be associated with surface quenching by external water (e.g., Büttner et al. 1999, 2002; Fitch et al. 2017; Hamilton et al. 2017).

Unit 1 contains beds with widely variable thicknesses and grain sizes, but all beds lie between bed 2.1 and talus, because no distinct beds were found during excavation into 6 m of talus and beach material below bed 1.1. Beds 1.1 through 1.7 ($\geq 150, 6, 2, 16, 1, 5, 7$ cm thick, respectively) are all planar, display sharp contacts, and are massive in structure. Beds 1.3 and 1.5 are both thin (2 and 1 cm thick, respectively), ash-rich beds displaying minor lapilli sag structures due to interstitial condensed water.

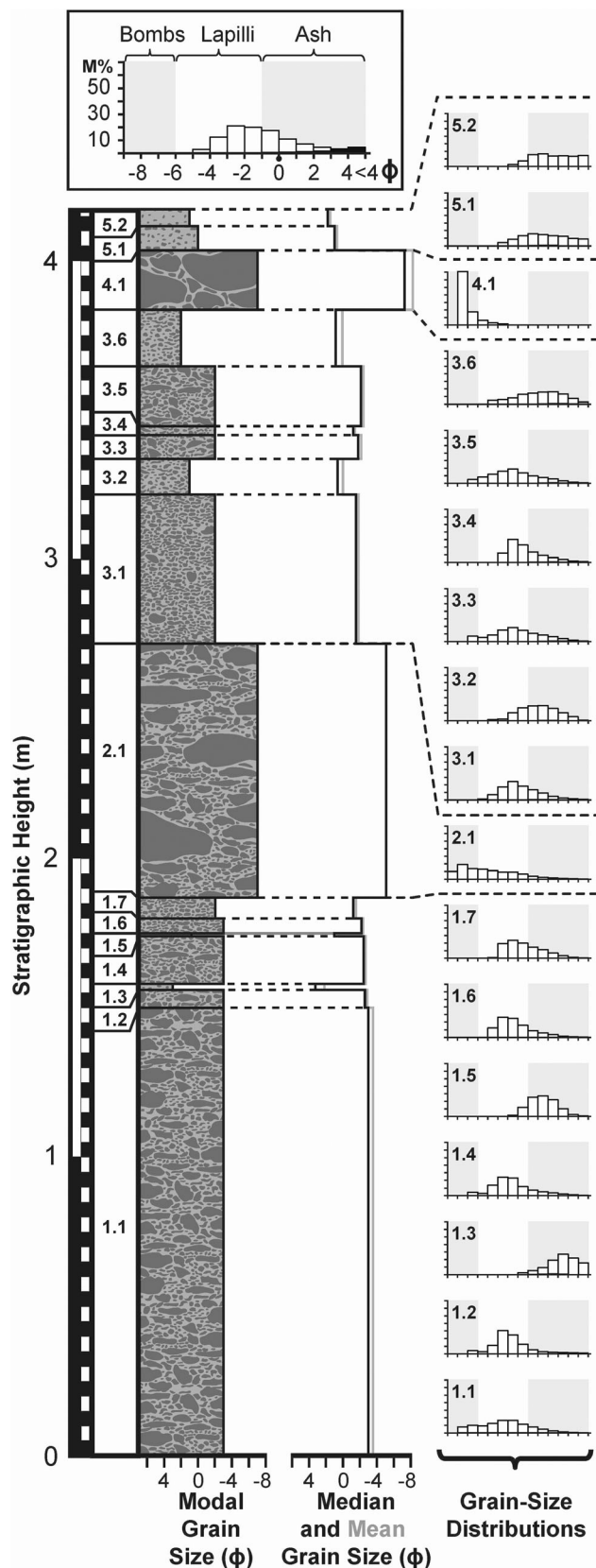


Fig. 5 Stratigraphic log of the Pu‘u Kīhōlo cone study section (17 beds) with bed grain size distributions, and modal, median, and mean grain sizes

Unit 2 is comprised of only one bed, 2.1 (85 cm thick), which is planar with sharp contacts, a massive structure, and is dominated by bomb- to coarse-lapilli-sized clasts. The largest clasts, typically up to 50 cm in diameter, are located near the middle of the bed, including a segmented, long (107 cm by 20 cm), dense spatter bomb.

Unit 3 contains beds with variable thicknesses and grain sizes (lapilli to ash dominated), but all beds lie between bomb- to coarse-lapilli-dominated beds 2.1 and 4.1. Beds 3.1 through 3.6 (50, 12, 8, 3, 20, and 19 cm thick, respectively) are all planar, display sharp contacts, and are massive in structure. Several large (30–60 cm), transitional (i.e., between pāhoehoe and ‘a‘ā characteristics) lava crustal blocks lie within unit 3, but associated beds could not be identified due to slumping and lack of access.

Unit 4 is comprised of only one bed, 4.1 (10–30 cm thick), which displays irregular contacts due to the fact that this bed is very coarse-grained (bomb dominated with 70 cm largest clast) with very little matrix material compared with that of beds 5.1 and 3.6, above and below. Bed 4.1 is planar, massive, and contacts are generally sharp.

Unit 5 consists of beds 5.1 and 5.2 (8 and 5.5 cm thick, respectively) which are ash-dominated and cover the cone surface. Beds are planar and massive, with sharp contacts. Bed 5.2 is distinctly brown to orange colored, and its top centimeter underwent post-emplacement cementation. Additionally, bed 5.2 displays irregular, decimeter scale fluted structures on the surface of the bed, and local, poorly preserved accretionary lapilli, both likely associated with condensed water in the ejecta envelope.

The Pu‘u Kīholo beds are finer grained on average than Rauðhólar beds (-3.9 and -4.5ϕ average median grain size, respectively; Hamilton et al. 2017). For beds at Pu‘u Kīholo with similar median grain size (and distribution shape) to Rauðhólar beds, the Pu‘u Kīholo beds contain a larger percentage of ash (Fig. 6).

Ejecta morphology and secondary fragmentation

Within any given bed, ash-sized grains contain greater proportions of blocky and shard-like grains, and smaller proportions of fluidal and spinose grains, than larger grain sizes (Fig. 7). This is consistent with the scale-dependent fragmentation behavior of grains observed at Rauðhólar (Fitch et al. 2017), which occurs because hydrodynamic fragmentation energy (which produces fluidal grains) increases exponentially with decreasing grain size, while brittle fragmentation energy increases linearly (Zimanowski et al. 2003; Dürig and Zimanowski 2012). This means that the production of blocky grains is energetically favored at fine grain sizes. Mossy ash-sized grains were only found in the 3.5–4 ϕ bin and make up $\leq 1\%$ of grains therein. Free crystals and cemented aggregates of ash-sized grains make up an average of only $4 \pm 3\%$ and $1 \pm 1\%$, respectively, of ash-sized ejecta.

In general, Pu‘u Kīholo beds are dominated by blocky grains, and over 80% of ash-sized grains exhibit blocky morphologies, compared with $< 65\%$ for Rauðhólar beds (Fig. 8(d)). The total mass percentage of blocky grains in Pu‘u Kīholo beds is roughly 40% greater than Rauðhólar beds, independent of bed median grain size (Fig. 9). Additionally, we found positive correlations between median grain size and both the percentage of blocky lapilli (moderate; $r^2 = 0.66$; Fig. 8(a)) and total mass percentage of blocky grains (strong; $r^2 = 0.85$; Fig. 9(a)). In comparison, Rauðhólar beds display less strong positive correlations between median grain size and total mass percentage of blocky grains (moderate; $r^2 = 0.67$; Fig. 9(a)) and the percentage of blocky ash (weak; $r^2 = 0.47$; Fig. 8(d)). These results indicate that brittle fragmentation is an important fragmentation mechanism at Pu‘u Kīholo, and furthermore, at both study sites, brittle fragmentation is of greater importance in more energetic explosions (which produce a finer median grain size). However, the

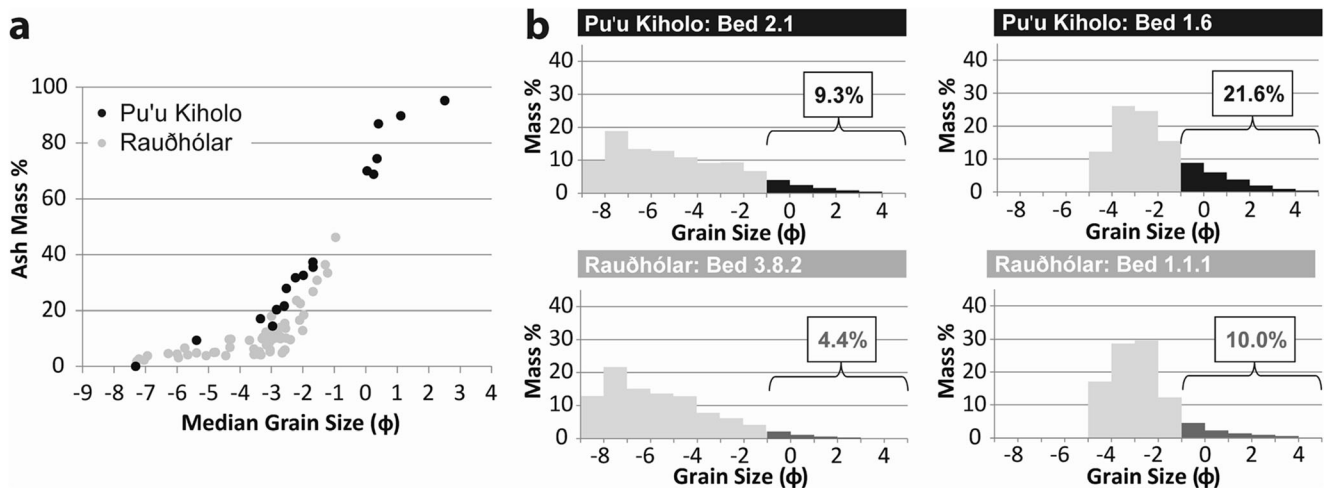


Fig. 6 (a) Ash mass percentages of Pu‘u Kīholo and Rauðhólar beds plotted against median grain size. (b) Total ash mass percentages for Pu‘u Kīholo and Rauðhólar beds with similar grain size distributions

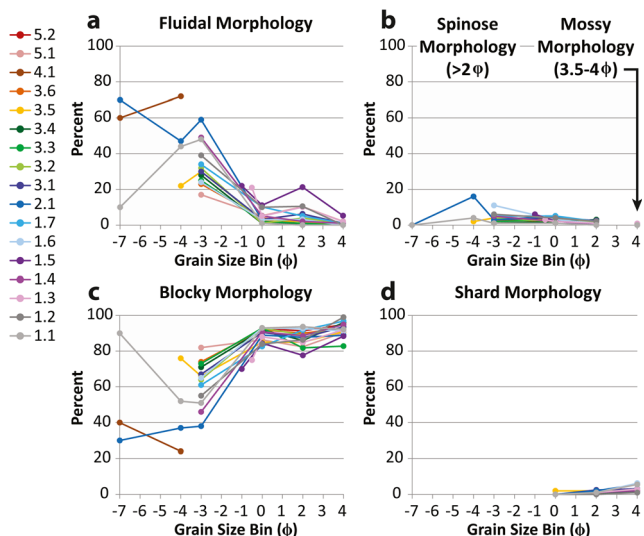


Fig. 7 Graphical depiction of relevant morphology results for bomb-, lapilli-, and ash-sized ejecta. The abscissa values correspond to the smallest size associated with the analyzed size range (i.e., grain size bin). For example, -3ϕ data points correspond with the -4 to -3ϕ range. On the ordinate, “percent” refers to the percentage out of 100 grains, except for bed 4.1 (-5 to -4ϕ ; 32–16 mm; 25 clasts total)

percentage of blocky lapilli displays a stronger correlation with median grain size at Pu’u Kīholo than the percentage of blocky ash, and the reverse is true for Rauðhólar. The abundance of fluidal ejecta follows similar, although negative, correlations as blocky ejecta, because the percentage of spinose ejecta displays negligible correlations with median grain size (Figs. 8 and 9).

At Pu’u Kīholo, many fluidal grains have undergone notable abrasion and/or breakage. An average of $67 \pm 11\%$ of fluidal lapilli-sized clasts have undergone brittle fragmentation over $> 50\%$ of their surfaces and $\geq 95\%$ of fluidal ash-sized grains are fragmented. At Rauðhólar, by comparison, only $5 \pm 6\%$ of fluidal lapilli-sized grains exhibit substantial abrasion or breakage surfaces and intact fluidal ash-sized grains are common.

Ejecta crystal textures and surface features

Three crystal textures were identified among lava–water explosion ejecta (Fig. 10(a)). Type 1 and type 2 textures are

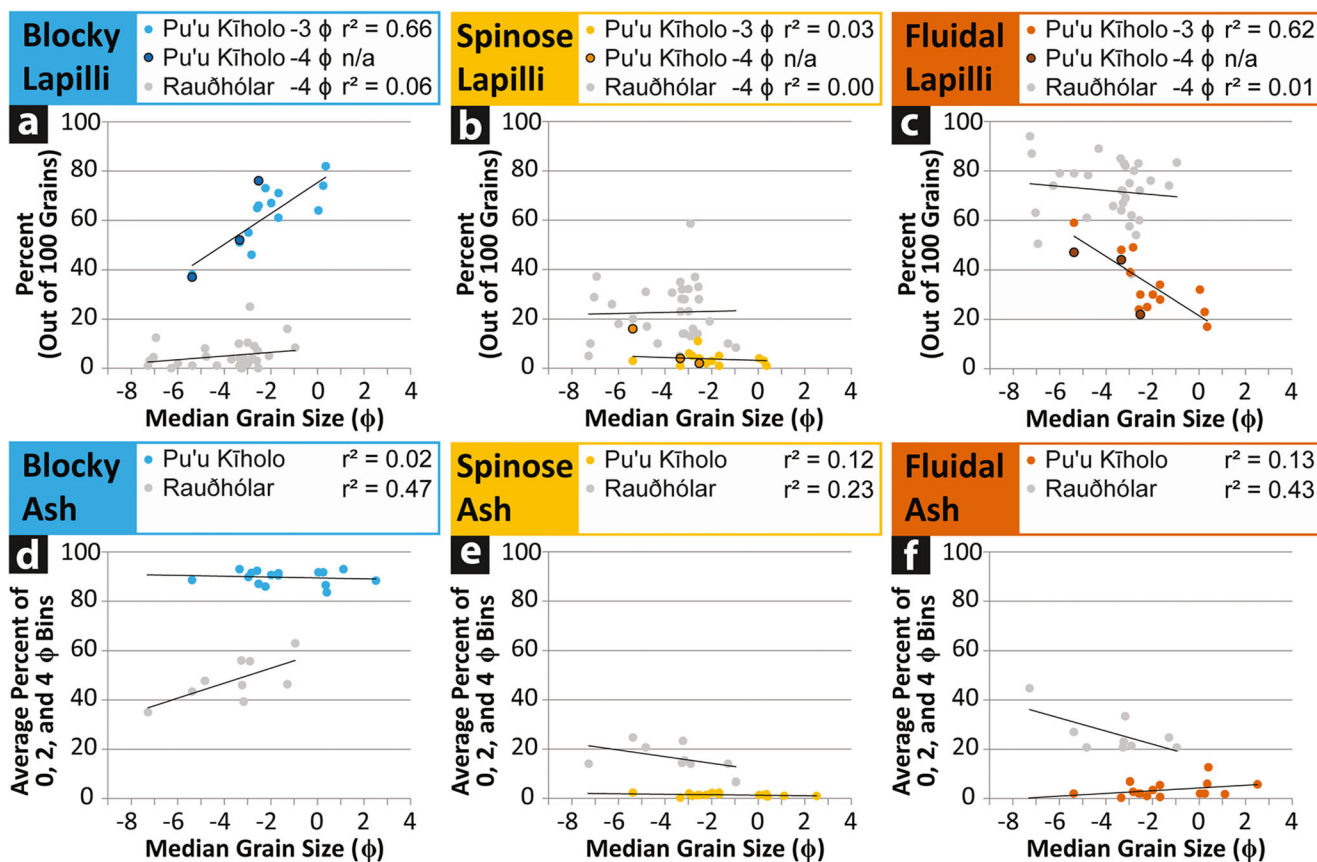


Fig. 8 Morphology results for lapilli- and ash-sized grains plotted against median grain size for each bed. (a) through (c) display the average percentage of the morphology type over 100 grains taken from the lapilli size ranges specified in key. Determination coefficients (r^2) were not calculated for the -4ϕ Pu’u Kīholo dataset but these data points lie within the

same range as the -3ϕ dataset. (d) through (f) display the average percentage (over the three size bins analyzed; 100 grains analyzed from each size bin) of the morphology type. Because the abscissa is logarithmic (ϕ), linear correlations are logarithmic correlations when associated with a linear (m) abscissa, with the same determination coefficient (r^2)

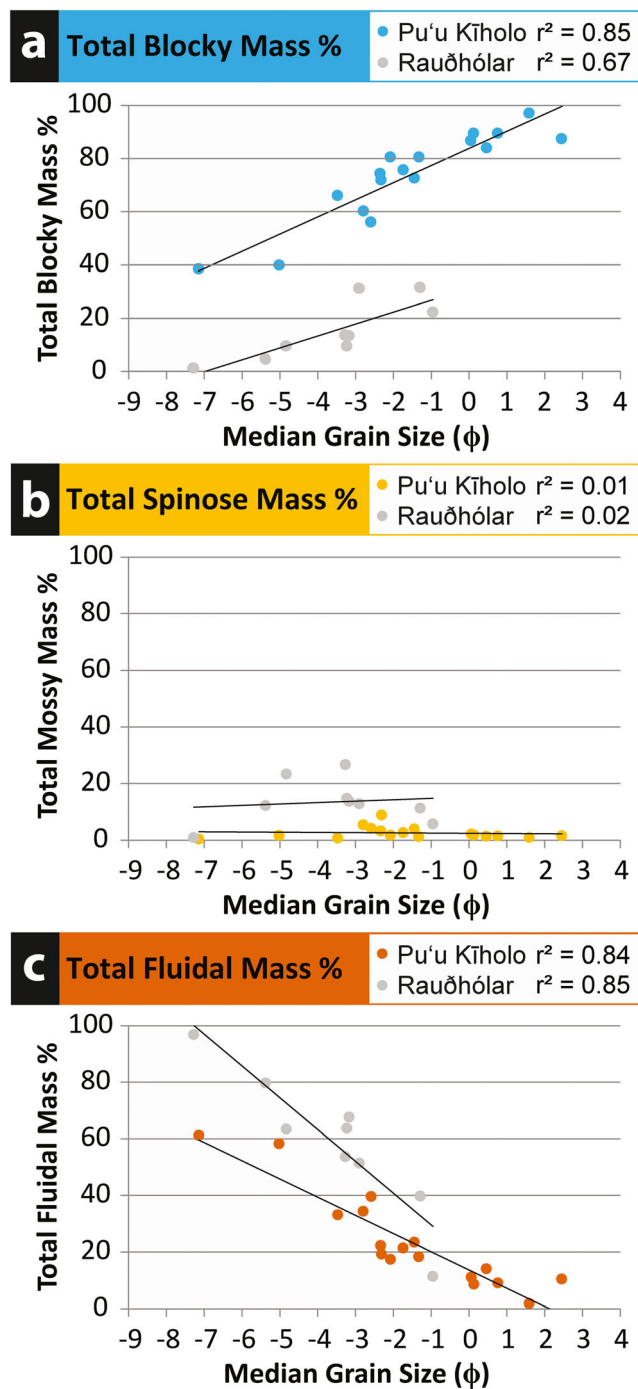


Fig. 9 For each bed, the total mass percentages (summed over all clast sizes) of blocky, spinose, and fluidal clasts are plotted against the median grain size of each associated bed. Because the abscissa is logarithmic (ϕ), linear correlations are logarithmic correlations when associated with a linear (m) abscissa, with the same determination coefficient (r^2)

holocrystalline (i.e., fully crystalline), containing olivine, pyroxene, feldspar, and oxides. These textures indicate lava cooled sufficiently slowly to form a crystalline groundmass and therefore solidified prior to fragmentation. Type 1 texture is associated with vesicular or dense lava lithics derived from transitional

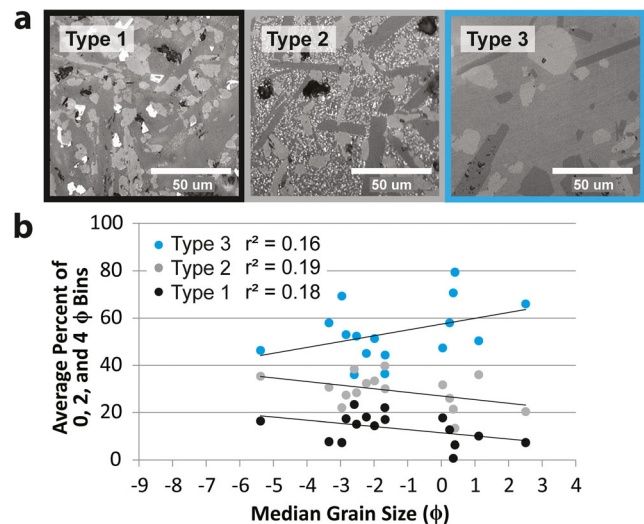


Fig. 10 (a) The three crystal textures identified among ash-sized lava–water explosion ejecta. Type 1 and type 2 textures are holocrystalline (i.e., fully crystalline) and type 3 texture is hypocrySTALLINE, containing 5–50% crystals (lighter and darker gray) within a glassy groundmass (middle-toned gray). (b) A plot of the average percentage (over the three size bins analyzed; 100 grains analyzed from each size bin) of each crystal texture type against the median grain size of each associated bed. Determination coefficient (r^2) values for all datasets are negligible, ranging from 0.16 to 0.19

flows (i.e., between pāhoehoe and ‘a‘ā characteristics), and type 2 texture forms below solid pāhoehoe crust, in coarse lapilli to bomb interiors, and in rubbly crustal fragments of transitional and ‘a‘ā flows. Type 3 grains are hypocrySTALLINE, containing 5–50% crystals of olivine, pyroxene, and feldspar within a glassy groundmass indicating that they fragmented from a source that cooled rapidly, such as the surfaces of ejecta and pāhoehoe lava flows, or the lava–water interface during MFCI (Fig. 1; Fitch et al. 2017). A gradational transition from type 3 to type 2 textures can occur over a thickness of ≤ 2 mm in pāhoehoe crustal profiles. The percentage of each type did not differ much over the three size bins examined for each bed, as indicated by a 4% average (and 10% maximum) standard deviation over all beds. Over the 17 beds analyzed, 36–79% (average of $54 \pm 12\%$) of ash-sized grains display type 3 texture, based on the average of the three size bins analyzed. Although there is a slight increase in the percentage of type 3 grains (out of 100 grains) with decreasing median grain size of the associated bed, we found a negligible correlation between these two values (Fig. 10(b)).

We analyzed the surface features of ash grains from two of the finest-grained beds, 1.3 and 1.5, and one of the coarsest-grained beds, 2.1, for comparison (Figs. 4 and 11(a)). We found that grains with stepped features and chemical surface pitting increase in abundance from the 1.5–2 ϕ (0.354–0.250 mm) fraction to the 3.5–4 ϕ (88–62 μm) fraction, often occur together, and make up to 70% and 50%, respectively, of blocky ash-sized grains within the bins analyzed. Polygonal quench cracks

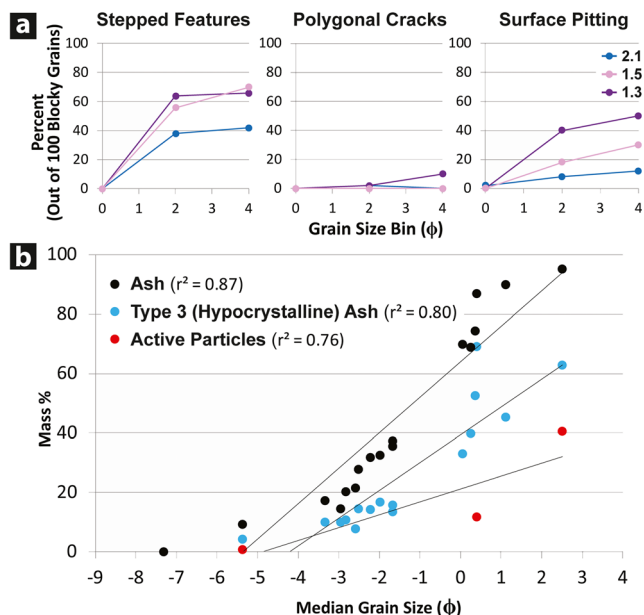


Fig. 11 (a) Results of the analysis of surface features associated with interaction with water: stepped features, polygonal quench cracks, and chemical surface pitting. Finer-grained beds 1.3 and 1.5, and coarse-grained bed 2.1, have been analyzed. For each bed, 50 ash-sized grains from each of three size bins were analyzed, which has been adjusted to reflect the inferred abundance over 100 grains, for comparison with other analyses. The abscissa values correspond to the smallest size associated with the analyzed size range (i.e., grain size bin). For example, 0 ϕ data points correspond to the -1.5 to 0 ϕ range. (b) The total ash (< 2 mm) mass percent (in black; also presented in Fig. 6), hypocrySTALLINE (type 3) ash (< 2 mm) mass percent in blue, and active particle (< 354 μm) mass percent in red, plotted against median grain size for each bed. Active particles are defined as mossy or blocky, where blocky grains are hypocrySTALLINE and display stepped features and/or quench cracks. Because the abscissa is logarithmic (ϕ), linear correlations are logarithmic correlations when associated with a linear (m) abscissa, with the same determination coefficient (r^2)

occur on $\leq 10\%$ of grains but are important indicators of MFCI. All three features are present in higher proportions in the ash from fine-grained beds 1.3 and 1.5, compared with that from the coarse-grained bed, 2.1. No stepped features, polygonal quench cracks, or chemical surface pitting were noted on grains from the 0.5 – 0 ϕ (1.41 – 1.00 mm) bin.

Based on our findings, we estimated the mass percentage of active particles as grains smaller than 1.5 ϕ (354 μm) that are mossy or blocky, where blocky grains are hypocrySTALLINE and display stepped features and/or polygonal quench cracks. We find that active particles make up 12% and 40% of the mass of the fine-grained beds 1.5 and 1.3, respectively, compared with 1% for coarse-grained bed 2.1 (Fig. 11(b)). The mass percentage of active particles, within the three beds for which this has been determined, displays a strong linear correlation with median grain size ($r^2 = 0.76$). The trend is somewhat similar to those of hypocrySTALLINE ash-sized grains ($r^2 = 0.80$) and all ash-sized grains ($r^2 = 0.87$) within all beds (Fig. 11(b)).

Lapilli vesicularity and component analysis

Using the morphology and vesicularity of known (archetypal) lava lithics from three sources, we are able to identify lava lithics from clasts derived from the molten core among Pu‘u Kīholo lapilli, based on the morphology (13 beds; 1300 clasts total) and vesicularity (Fig. 12; 5 beds; 395 clasts total) analyses performed on these ejecta (Fig. 13). Lava lithics, derived from the brittle and visco-elastic layer of the lava crust, display blocky morphology, except where clasts retain a smooth pāhoehoe crustal surface. Outer pāhoehoe crust displays homogeneously sized and dispersed bubbles and a mean vesicularity of $57 \pm 4\%$ (7 archetypal clasts). Conversely, the underlying middle and inner visco-elastic layers have mean vesicularities of $30 \pm 4\%$ (3 archetypal clasts) and $4 \pm 4\%$ (3 archetypal clasts), respectively. The majority of blocky lapilli at Pu‘u Kīholo have vesicularities $< 30\%$ (Fig. 12), with a mean of $25 \pm 14\%$ (214 clasts). Lapilli derived from the molten core of the lava flow display fluidal or spinose (viscous) morphologies and contain heterogeneously sized bubbles. The majority of fluidal and spinose lapilli at Pu‘u Kīholo have vesicularities $> 30\%$ (Fig. 12), with mean values of $34 \pm 11\%$ (152 clasts) and $35 \pm 9\%$ (29 clasts), respectively. Only 13% of fluidal clasts derived from the molten core have very low vesicularities ($< 20\%$). Based on these results, it is likely that for blocky lapilli (1) the 38% of clasts with $> 20\%$ vesicularity are mostly lava lithics, (2) the 57% of clasts with 20 – 50% vesicularity are mostly fluidal or spinose clasts that have undergone significant breakage and/or abrasion, and (3) the 5% of clasts with $> 50\%$ vesicularity are mostly pāhoehoe outer crust. Therefore, at Pu‘u Kīholo, not all blocky lapilli are lava lithics and the percentage of lapilli sourced from the interior makes up more than just the fluidal and spinose lapilli.

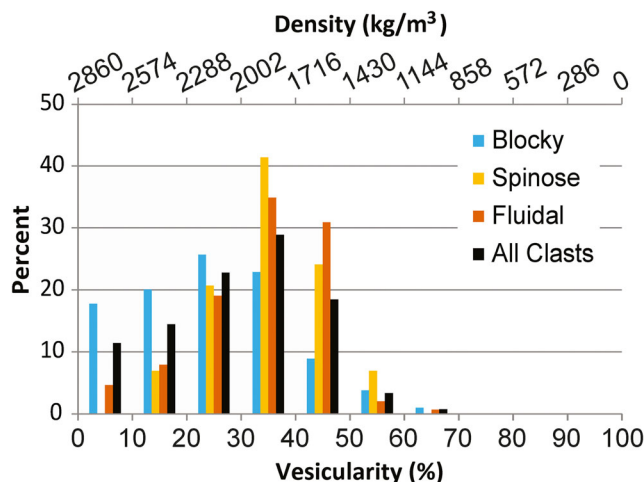


Fig. 12 Vesicularity histograms of all 395 clasts analyzed from Pu‘u Kīholo cone, showing the relative contributions of blocky, spinose, and fluidal clasts. On the ordinate, “percent” refers to the percentage of clasts out of the total number analyzed for each morphology, with a total of 214, 29, and 152 clasts of blocky, spinose, and fluidal morphologies, respectively

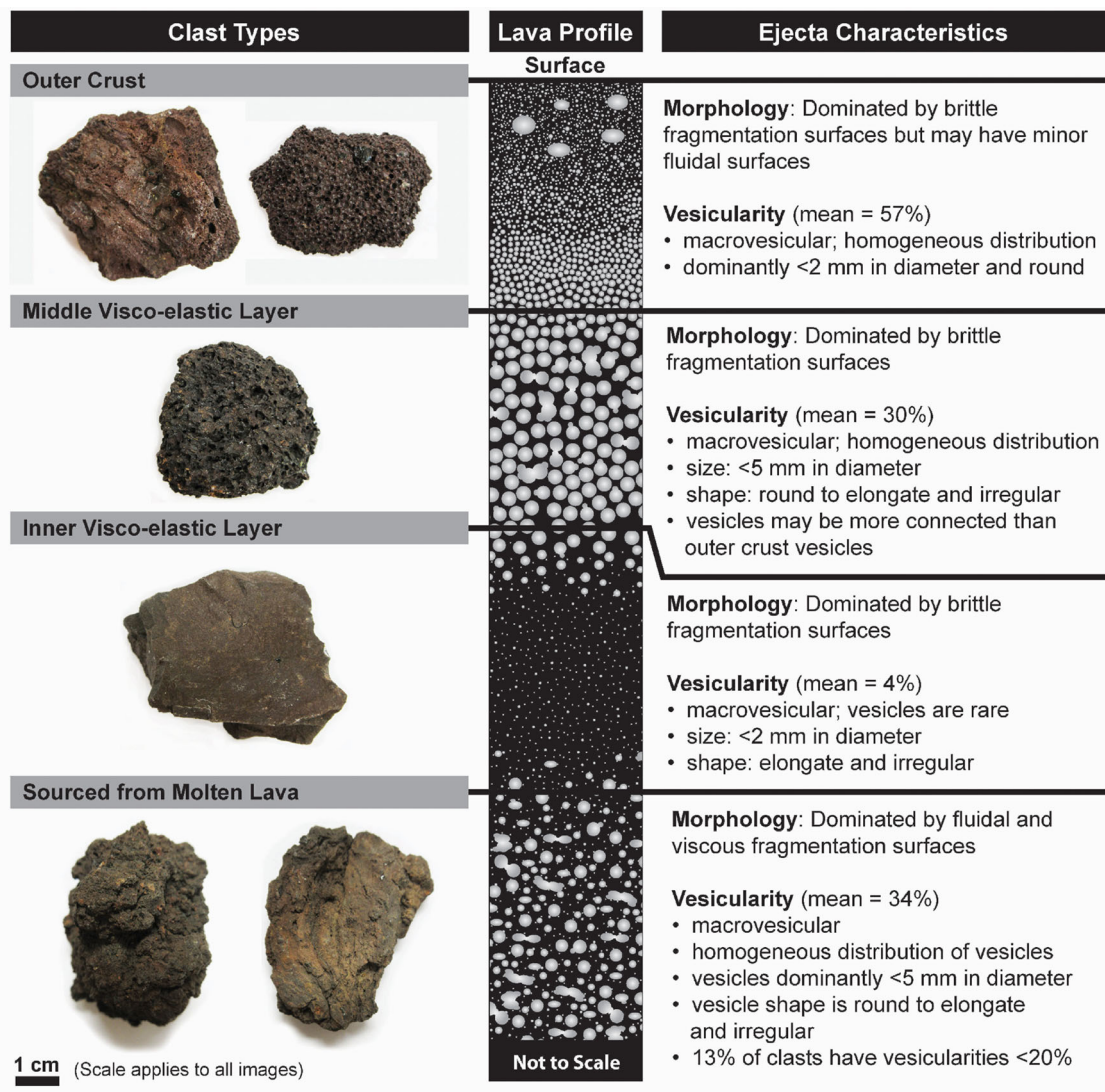


Fig. 13 Ejectasource material classifications based on morphology and vesicularity analysis. A schematic lava profile is shown for comparison, with vesicle (white) abundances and characteristics found in the corresponding ejecta

Discussion

Lava flow behavior

Ejecta characteristics at Pu‘u Kīholo and Rauðhólar enable us to better constrain the properties and behavior of lava associated with rootless cone formation. At Rauðhólar, which is associated with tube-fed pāhoehoe, the percentage of blocky lapilli-sized clasts is consistently low (average of $5 \pm 5\%$), and correlations between median grain size and blocky, fluidal, and spinose lapilli-sized clasts are negligible (Fig. 8). In a tube-fed pāhoehoe system, the solid upper crust is not mechanically coupled to the lava within the tube (cf. Kauahikaua et al. 1998). Therefore, we infer that after the original lava tube crust is removed during the initiation of explosive activity, subsequent explosions contain very little lava lithic material. In contrast, at Pu‘u Kīholo, the percentage

of blocky lapilli correlates strongly with median grain size (Fig. 8), and the total mass percentages of blocky clasts are consistently higher as well (Fig. 9), which indicates that explosions expanded through a lava profile that included a crust during every explosion. Therefore, the crust was likely mechanically coupled to the molten lava, consistent with lava flowing in a channel (cf. Kauahikaua et al. 1998), which is common in the Hapaimanu flow field and on the Mauna Loa south flank coastal plain in general.

Previous workers have suggested that flows with disrupted crusts may be more susceptible to explosive interactions because of greater crustal permeability (Moore and Ault 1965; Fisher 1968; Mattox and Mangan 1997). Considering the abundant evidence for wide channels, ponding, and high lava flux among Hapaimanu flows, it is likely that flows associated with the Na Pu‘u a Pele cones, including Pu‘u Kīholo, also experienced crustal disruption. Lava lithic characteristics at

Pu‘u Kīholo are consistent both with surrounding transitional, rumbly pāhoehoe flows, and lava lithics from a small spatter-rich cone associated with a transitional flow. Additionally, the prevalence of embedded clasts and armored bombs with lava lithic cores (see Fig. 13 for lava lithic characteristics) may indicate pre-explosion core–crust mixing.

Lava–water mixing conditions

Based on the preservation of a partial ring of ejecta, explosions at Pu‘u Kīholo may have originated at what was a discrete inland location, or closely spaced set of locations, near the present cone center (Fig. 14(a)). In this scenario, fracture (but not collapse) of the water-saturated bench of lava fragments and flows (i.e., lava delta) underlying the active flow brought molten lava into contact with water, known as “confined mixing” (Mattox and Mangan 1997), initiating explosions (Fig. 1 (phase 4a) and Fig. 14b). This model is consistent with the observations of two circular littoral rootless cones on the island of Hawai‘i with large crater rim radii,

ranging from 100 to 130 m, associated with tube-fed pāhoehoe flows with high volumetric flow rates (Jurado-Chichay et al. 1996). Alternatively, explosions at Pu‘u Kīholo may have also originated at the ocean entry, with a partial ring of ejecta deposited on an irregularly shaped shoreline (Fig. 14(c, d)). In this scenario, explosions were likely initiated by vigorous mixing of lava and water due to high lava flux and wave action, referred to as “open mixing” (Mattox and Mangan 1997) (Fig. 1 (phase 4b)).

Hamilton et al. (2017) identified alternating finer- and coarser-grained beds at Rauðhólar, interpreted to be associated with a higher-energy opening phase of an explosion followed by a lower-energy phase, continuing until water availability diminished. However, at Pu‘u Kīholo, we do not see stratigraphic patterning or grading in beds and, therefore, a combination of variable lava flux and variable crustal permeability at the flow base, in the presence of unlimited water, likely controlled the degree of lava–water mixing and explosion energy.

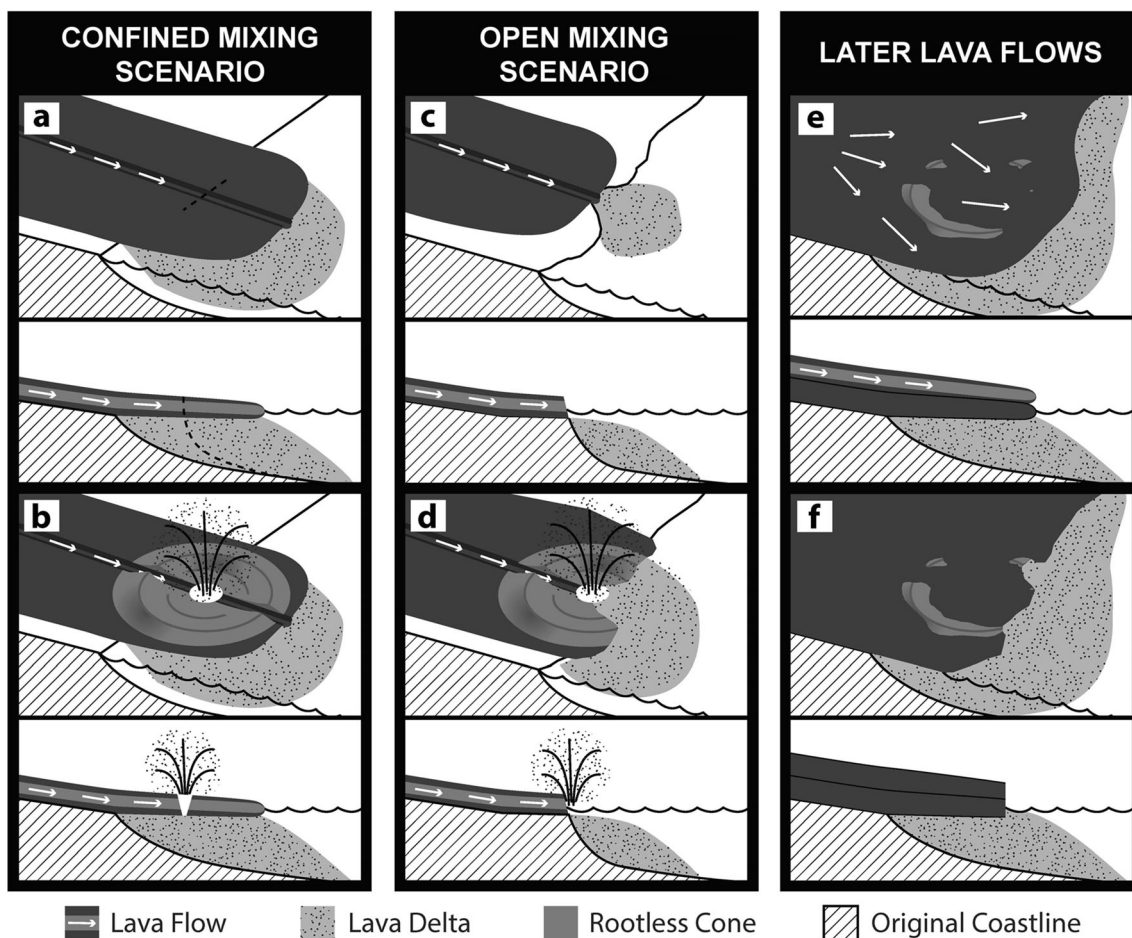


Fig. 14 Possible formation scenarios of Pu‘u Kīholo cone. In a confined mixing scenario, (a) fracturing the base of the lava flow causes molten lava to come into contact with water within the lava delta, resulting in (b) vigorous mixing and explosive detonation. In an open mixing scenario, (c) lava enters the ocean and (d) explosions are initiated by vigorous

premixing of lava and water due to high lava flux and wave action. After Pu‘u Kīholo cone was formed, later, lava flows (e) inundated the area, surrounding and partially overtopping the cone, with (f) subsequent collapse and erosion of the lava delta to produce the current coastline dominated by vertical cliffs

Ash formation mechanisms

Compared with Rauðhólar beds with similar median grain sizes, Pu'ū Kīholo beds contain a larger mass percentage of ash-sized grains, even though the study section is upwind of the explosion site. The average percentage of blocky ash-sized grains in particular is consistently higher for Pu'ū Kīholo beds ($90 \pm 3\%$) than Rauðhólar beds ($48 \pm 9\%$), in agreement with previous work on higher-energy MFCIs (Büttner and Zimanowski 1998). However, almost three-quarters of fluidal lapilli-sized clasts are dominated by secondary fragmentation surfaces, including fine-scale abrasion. Therefore, collisions among clasts during transport and deposition, in addition to turbulent shedding of cooled rinds, may also produce blocky ash-sized grains (Mastin 2007; Manga et al. 2011).

Previous work on lava–water explosions found that hypocrySTALLINE, blocky ash-sized grains can form at the interface between lava and water, and they are interpreted to be active particles (Fitch et al. 2017), especially those that have specific surface features (this study). We therefore expect that as explosion energy increases, the abundance of active particles produced also increases. Correspondingly, we find that surface features associated with active particles are more abundant among grains from finer-grained beds (Fig. 11(a)) and we find a strong linear correlation between active particle mass percentage and median grain size (a proxy for explosion energy) (Fig. 11(b)). Active particles associated with MFCI experiments are inferred to be smaller than 3ϕ ($125 \mu\text{m}$; Heiken and Wohletz 1985; Wohletz 1986; Büttner et al. 1999, 2002), because the abundance of these very fine ash-sized grains is greater in experimental MFCIs, compared with experimental explosions driven by expanding gas only. However, we found grains with active particle characteristics in the $1.5\text{--}2 \phi$ ($354\text{--}250 \mu\text{m}$) size bin. This highlights the importance of analyzing ash beyond an assumed size range to determine the range of active particle characteristics present over different systems.

Fluidal ash-sized grains, though not abundant at Pu'ū Kīholo, may provide additional insights into explosion processes. A notable secondary peak of fluidal ash percentage in the $1.5\text{--}2 \phi$ ($354\text{--}250 \mu\text{m}$) size bin occurs in beds 1.3 and 1.5, two of the finest-grained beds in the section (Fig. 7(a)). This secondary peak, composed of micro-spatter and Pele's hair, may result from greater fragmentation energy (per unit mass) (Zimanowski et al. 2003) and higher ejection velocities (Zimanowski et al. 1997a, 2015; Büttner et al. 2002; Grunewald et al. 2007).

Conclusions

Based on the structural, stratigraphic, and lava lithic characteristics of Pu'ū Kīholo cone, we infer that its formation was associated with the interaction of a channelized, transitional, rubbly pāhoehoe flow with water either (1) from within the underlying

lava delta or (2) at the shoreline during ocean entry (Figs. 1 and 14). Lava–water interactions at Pu'ū Kīholo occurred under conditions of higher lava flux, more vigorous water influx and mixing, and an abundance of water, and these factors contributed to the generation of more energetic explosions (e.g., Wohletz and McQueen 1984; Zimanowski et al. 1997b; Jurado-Chichay et al. 1996; Mattox and Mangan 1997) on average compared with Rauðhólar. Higher explosion energy at Pu'ū Kīholo, compared with Rauðhólar, contributed to the greater (1) degree of fragmentation of the lava, producing beds with finer median grain sizes on average, and (2) dispersal of ejecta, producing an uncommonly large-diameter rootless cone (Greeley and Fagents 2001; Fagents and Thordarson 2007).

Beds generated by higher-energy explosions display finer grain sizes and the finest-grained beds at Pu'ū Kīholo, 1.3, 1.5, 5.1, and 5.2, have median grain sizes ranging from $0.4\text{--}2.5 \phi$ ($0.6\text{--}0.2 \text{ mm}$). Based on the presence of lapilli sag structures (beds 1.3 and 1.5), fluted surface structures, accretionary lapilli (bed 5.2), and enhanced chemical surface pitting (only analyzed for beds 1.3 and 1.5), these beds preserve evidence of condensed water in the ejecta envelope that was either not preserved or not abundant in coarser-grained beds, due to the scarcity of water and low production of fines (cf. Mattox and Mangan 1997). These fine-grained beds also have the highest mass percentage of blocky grains, especially blocky ash-sized grains. Although all beds contain ash-sized ejecta formed by secondary fragmentation, the average percentage of hypocrySTALLINE (type 3) ash-sized grains in these beds is slightly higher ($67 \pm 12\%$) than for coarser-grained beds ($50 \pm 9\%$) and both the percentage, out of one hundred grains, and the mass percentage of active particles for beds 1.3 and 1.5 are higher than coarser-grained bed 2.1. Furthermore, we find active particle characteristics over slightly larger ash grains than previous work; therefore, it is important to analyze a broader range of ash sizes to identify active particles in natural systems.

This study provides additional insight into the processes associated with lava–water explosions and the characteristics of the resulting ejecta, especially for those produced by higher-energy explosions. Taken together, Fitch et al. (2017) and this work catalog fragmentation mechanisms of lava–water ejecta over a range of grain sizes, for a total of 85 rootless beds with median grain sizes ranging from -7.2 to 2.5ϕ (155 to $176 \mu\text{m}$). This work paves the way for energy modeling of lava–water explosions, which may then be used to understand and quantify processes occurring during magma–water interactions, allowing us to better constrain the energetics of hydrovolcanic eruptions.

Acknowledgments We would like to thank the Hawai'i Department of Land and Natural Resources for the access to the study area, which required a permit. We are grateful to Gary Huss, Phillip Ooi, Elizabeth Koeman-Shields, and Jessica Galacgac for the instrumentation access and training. This work was improved by discussions with Frank Trusdell, Don Swanson, Bruce Houghton, Scott Rowland, and Carolyn Parcheta. We acknowledge journal reviews by Alison Graettinger, an

anonymous reviewer, and associate editor Pierre-Simon Ross. Lastly, this work could not have been done without the field assistance and good company of Jenn Randell-Tamaariki and Bryant Quinonez-Servin.

Funding information This work was supported by the University of Hawai'i Bullard Fellowship and HIGP (publication number 2416) and SOEST (publication number 11018).

References

- Blott SJ, Pye K (2001) GRADISTAT: a grain size distribution and statistics package for the analysis of unconsolidated sediments. *Earth Surf Process Landf* 26(11):1237–1248
- Büttner R, Zimanowski B (1998) Physics of thermohydraulic explosions. *Phys Rev E* 57(5):5726–5729
- Büttner R, Dellino P, Zimanowski B (1999) Identifying magma–water interaction from the surface features of ash particles. *Nature* 401(6754):688–690
- Büttner R, Dellino P, La Volpe L, Lorenz V, Zimanowski B (2002) Thermohydraulic explosions in phreatomagmatic eruptions as evidenced by the comparison between pyroclasts and products from molten fuel coolant interaction experiments. *Journal of Geophysical Research: Solid Earth* 107(B11):5–14
- Colgate SA, Sigurgeirsson T (1973) Dynamic mixing of water and lava. *Nature* 244(5418):552–555
- Dürig T, Zimanowski B (2012) “Breaking news” on the formation of volcanic ash: fracture dynamics in silicate glass. *Earth Planet Sci Lett* 335:1–8
- Dürig T, Sonder I, Zimanowski B, Beyrichen H, Büttner R (2012) Generation of volcanic ash by basaltic volcanism. *J Geophys Res: Solid Earth* 117(B1). <https://doi.org/10.1029/2011JB008628>
- Fagents SA, Thordarson T (2007) Rootless volcanic cones in Iceland and on Mars. In: Chapman MG (ed) *The geology of Mars: evidence from earth-based analog*. Cambridge University Press, United Kingdom, pp 151–177
- Fisher RV (1968) Pu'u Hou littoral cones, Hawaii. *Geol Rundsch* 57(3): 837–864
- Fitch EP, Fagents SA, Thordarson T, Hamilton CW (2017) Fragmentation mechanisms associated with explosive lava–water interactions in a lacustrine environment. *Bull Volcanol* 79(1). <https://doi.org/10.1007/s00445-016-1087-3>
- Folk RL, Ward WC (1957) Brazos River bar: a study in the significance of grain size parameters. *J Sediment Petrol* 27:3–26
- Greeley R, Fagents SA (2001) Icelandic pseudocraters as analogs to some volcanic cones on Mars. *Journal of Geophysical Research: Planets* 106(E9):20527–20546
- Grunewald U, Zimanowski B, Büttner R, Phillips LF, Heide K, Büchel G (2007) MFCI experiments on the influence of NaCl-saturated water on phreatomagmatic explosions. *J Volcanol Geotherm Res* 159(1–3):126–137
- Hamilton CW, Fitch EP, Fagents SA, Thordarson T (2017) Rootless tephra stratigraphy and emplacement processes. *Bull Volcanol* 79(1). <https://doi.org/10.1007/s00445-016-1086-4>
- Harris AJ, Rowland SK (2015) Lava flows and rheology. In: Sigurdsson H, Houghton B, McNutt S, Rymer H, Stix J (eds) *The Encyclopedia of Volcanoes*. Academic Press, pp 321–342
- Heiken G, Wohletz K (1985) *Volcanic ash*. University Press, California, Chicago, Harvard & MIT
- Horwell CJ (2007) Grain-size analysis of volcanic ash for the rapid assessment of respiratory health hazard. *J Environ Monit* 9(10):1107–1115
- Houghton B, Hackett W (1984) Strombolian and phreatomagmatic deposits of Ohakune Craters, Ruapehu, New Zealand: a complex interaction between external water and rising basaltic magma. *J Volcanol Geotherm Res* 21(3):207–231
- Houghton B, Schmincke H (1986) Mixed deposits of simultaneous strombolian and phreatomagmatic volcanism: Rothenberg volcano, East Eifel volcanic field. *J Volcanol Geotherm Res* 30(1):117–130
- Houghton BF, Wilson CJN (1989) A vesicularity index for pyroclastic deposits. *Bull Volcanol* 51(6):451–462
- Jurado-Chichay Z, Rowland SK, Walker GP (1996) The formation of circular littoral cones from tube-fed pāhoehoe: Mauna Loa, Hawai'i. *Bull Volcanol* 57(7):471–482
- Kauahikaua J, Cashman KV, Mattox TN, Heliker CC, Hon KA, Mangan MT, Thornber CR (1998) Observations on basaltic lava streams in tubes from Kilauea Volcano, island of Hawai'i. *Journal of Geophysical Research: Solid Earth* 103(B11):27303–27323
- Lorenz V (1987) Phreatomagmatism and its relevance. *Chem Geol* 62(1–2):149–156
- Manga M, Patel A, Dufek J (2011) Rounding of pumice clasts during transport: field measurements and laboratory studies. *Bull Volcanol* 73(3):321–333
- Mastin LG (2007) Generation of fine hydromagmatic ash by growth and disintegration of glassy rinds. *J Geophys Res: Solid Earth* 112(B2): <https://doi.org/10.1029/2005JB003883>
- Mattox TN, Mangan MT (1997) Littoral hydrovolcanic explosions: a case study of lava–seawater interaction at Kilauea volcano. *J Volcanol Geotherm Res* 75(1–2):1–17
- Moore JG, Ault WU (1965) Historic littoral cones in Hawaii. *Pac. Sci.* XIX 1:3–11
- Morrissey M, Zimanowski B, Wohletz K, Büttner R (2000) Phreatomagmatic fragmentation. In: Houghton B, Rymer H, Stix J, McNutt S (eds) *Encyclopedia of volcanoes*. Academic Press, San Diego, pp 431–445
- Rowland SK, Walker GP (1987) Toothpaste lava: characteristics and origin of a lava structural type transitional between pāhoehoe and aa. *Bull Volcanol* 49(4):631–641
- Sheridan MF, Wohletz KH (1983) Hydrovolcanism: basic considerations and review. *J Volcanol Geotherm Res* 17(1–4):1–29
- Sonder I, Harp AG, Graettinger AH, Moitra P, Valentine GA, Büttner R, Zimanowski B (2018) Meter-scale experiments on magma–water interaction. *Journal of Geophysical Research: Solid Earth* 123(12): 10–597
- Trusdell FA, Lockwood JP (in press) Geologic map of the lower-southwest rift zone of Mauna Loa Volcano, Island of Hawai'i, Hawaii: U.S. Geological Survey SIM 2932-C, scale 1:50,000
- Von Komorowicz M (1912) *Vulkanologische studien auf einigen inseln des Atlantischen Oceans*. E. Schweizerbart, Stuttgart, Germany
- Westervelt WD (1916) *Hawaiian legends of volcanoes*. Ellis Press
- Wohletz KH (1983) Mechanisms of hydrovolcanic pyroclast formation: grain-size, scanning electron microscopy, and experimental studies. *J Volcanol Geotherm Res* 17(1–4):31–63
- Wohletz KH (1986) Explosive magma–water interactions: thermodynamics, explosion mechanisms, and field studies. *Bull Volcanol* 48(5):245–264
- Wohletz KH, McQueen R (1981). Experimental hydromagmatic volcanism. *Amer. Geophys. Union Trans., EOS* 62(45):1085
- Wohletz KH, McQueen RG (1984) Experimental studies of hydromagmatic volcanism. In: *Explosive volcanism: inception, evolution, and hazards*. Studies in geophysics. National Academy Press, Washington, DC. pp 158–169
- Wohletz KH, Zimanowski B, Büttner R (2013) Magma–water interactions. In: Fagents SA, Gregg TKP, Lopes RMC (eds) *Modeling volcanic processes*. Cambridge University Press, New York, pp 230–257
- Xie S-P, Liu WT, Liu Q, Nonaka M (2001) Far-reaching effects of the Hawaiian Islands on the Pacific Ocean-atmosphere system. *Science* 292(5524):2057–2060

- Zimanowski B (2001) Phreatomagmatic explosions. In: Freundt A, Rosi M (eds) From magma to tephra: modeling physical processes of explosive volcanic eruptions, developments in volcanology 4. Elsevier Science B.V, Amsterdam, The Netherlands, p 336
- Zimanowski B, Büttner R, Lorenz V, Häfele H-G (1997a) Fragmentation of basaltic melt in the course of explosive volcanism. *Journal of Geophysical Research: Solid Earth* 102(B1):803–814
- Zimanowski B, Büttner R, Lorenz V (1997b) Premixing of magma and water in MFCI experiments. *Bull Volcanol* 58(6):491–495
- Zimanowski B, Wohletz K, Dellino P, Büttner R (2003) The volcanic ash problem. *J Volcanol Geotherm Res* 122(1):1–5
- Zimanowski B, Büttner R, Dellino P, White JD, Wohletz KH (2015) Magma-water interaction and phreatomagmatic fragmentation. In: Houghton B, McNutt S, Rymer H, Stix J (eds) Sigurdsson H. Academic Press, *The Encyclopedia of Volcanoes*, pp 473–484